Вісник Тернопільського національного технічного університету
https://doi.org/10.33108/visnyk_tntu
Scientific Journal of the Ternopil National Technical University
2025, № 2 (118) https://doi.org/10.33108/visnyk_tntu2025.02
ISSN 2522-4433. Web: ***visnyk.tntu.edu.ua***

UDC 539.3

ON DEFORMATION PECULIARITIES OF TWO THIN STRIPS WITH A MICROCRACK AT THE INTERFACE

Oleksandr Kletskov[1]; Valentine Silich-Balhabaieva[1]; Alla Sheveleva[1]; Volodymyr Loboda[1]; Yuri Lapusta[2]

[1]Oles Honchar Dnipro National University, Dnipro, Ukraine
[2]Université Clermont Auvergne, Clermont Auvergne INP, SIGMA Clermont, CNRS, Institut Pascal, Clermont-Ferrand, F-63000, France

Abstract. *This study examines the problem of plane strain in a crack between two isotropic, linearly elastic layers, one of which is rigidly fixed. The Fourier integral transform method was applied, reducing the initial system of differential equations to a system of ordinary differential equations. A system of singular integral equations (SIE) was constructed to satisfy the boundary conditions of the problem. By discretizing this system, it was further reduced to a system of linear algebraic equations (SLAE).*

Analytical expressions were obtained for the crack opening and stress distribution along the interface, allowing the calculation of the energy release rate (ERR) at the crack tips. A numerical illustration of the results was conducted, including graphs of crack opening and stress dependence for various layer thicknesses and Young's moduli.

Comparison between analytical and numerical solutions, obtained using the finite element method (FEM), showed good agreement for the case of a microcrack with variable characteristics of the thin coating and the lower layer. A significant influence of the coating thickness on the energy release rate was identified.

Key words: *microcrack, stress-strain state, singular integral equations, energy release rate, crack opening.*

https://doi.org/10.33108/visnyk_tntu2025.02.153 *Received 14.03.2025*

1. INTRODUCTION

In modern materials science, where thin films and overlays are widely used to reinforce and protect structures, the reliability of connections between such coatings and base materials remains a crucial aspect. These connections often suffer from microcracks at layer interfaces, which can compromise the integrity of the structure and reduce its operational performance. Microcracks at the boundary between two thin strips or a strip and an overlay become critical as they serve as zones of concentrated stress, which promotes further material degradation. Understanding the deformation behavior and the impact of microcracks at these interfaces is essential for predicting the reliability of complex multilayered systems.

Investigation of cracks forming at the fixed edges of thin strips is of particular interest, as such defects can cause local stress distribution changes, affecting the stability and strength of the structure. Analyzing the interaction between a thin strip and an overlay, taking into account the presence of a microcrack at their connection, deepens the understanding of micro-level fracture processes and helps develop approaches to prevent them.

Many studies have examined cracks between two materials, with recent publications focusing on different types of stress-strain states, materials, loading conditions, and crack

Corresponding author: Oleksandr Kletskov; e-mail: alex.kl87@i.ua

geometries [1–5]. Studies on cracks in homogeneous and heterogeneous strips are especially notable. In particular, work [6] analyzes the stress-strain state of three heterogeneous materials with internal and interphase cracks. Crack investigation in a nonhomogeneous medium with a constant Poisson's ratio and an exponentially varying Young's modulus is covered in [7], while [8] explores cases where one material has nonhomogeneous properties in the interaction zone. Study [9] examines a central crack in an infinite strip under internal pressure and concentrated forces at its edges. It is important to note that these studies primarily address internal and interfacial macrocracks. Interaction of an electrode with an electrically conductive interface crack was considered in [10] and an analysis of pre-fracture zones for an electrically permeable crack in an interlayer between piezoelectric materials has been performed in [11]. The works [12–14] are devoted to the study of cracks and contact problems taking into account the elastic-plastic behavior of materials.

This work focuses on the stress-strain analysis in the zone of a microcrack at the boundary between two isotropic layers of different thicknesses, with one layer rigidly fixed. This analysis provides essential information on the deformation behavior of multilayered structures with cracks, which can improve designs of structures including thin films and overlays under different mechanical loads.

2. EXPERIMENTAL METHODS

Consider the problem of plane deformation of a crack $|x| \le b$ between two isotropic, linearly elastic, infinite layers of thickness h_1 and h_2, with the lower layer rigidly fixed $y = -h_2$. The crack is assumed to be open due to uniform internal pressure p_0 applied to its edges (Fig. 1).

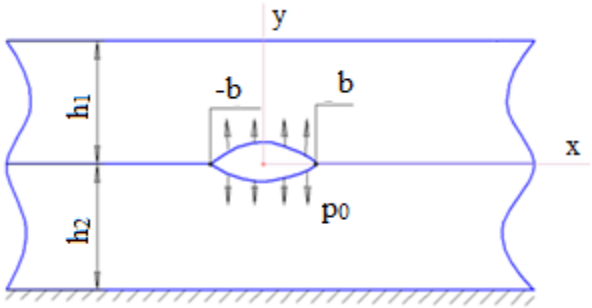

Figure 1. The geometry and load of the problem

To solve this problem, it is necessary to solve a boundary value problem, which is described by a system of second-order partial differential equations p0

$$\mu_i \, \Delta^2 u^{(i)}(x,y) + \frac{2\mu_i}{\kappa_i - 1} \frac{\partial}{\partial x}\left(\frac{\partial u^{(i)}(x,y)}{\partial x} + \frac{\partial v^{(i)}(x,y)}{\partial y} \right) = 0, \qquad (1)$$

$$\mu_i \, \Delta^2 v^{(i)}(x,y) + \frac{2\mu_i}{\kappa_i - 1} \frac{\partial}{\partial x}\left(\frac{\partial u^{(i)}(x,y)}{\partial x} + \frac{\partial v^{(i)}(x,y)}{\partial y} \right) = 0, \qquad (2)$$

where μ_i and ν_i are the shear modulus and Poisson's ratio, respectively, $i = 1, 2$,

$$\kappa_i = \begin{cases} 3-4\nu_i & \text{– for plane deformation,} \\ \dfrac{3-\nu_i}{1+\nu_i} & \text{– for the plane stress state.} \end{cases}$$

The boundary conditions due to symmetry, can be written as:

$$\tau_{xy}^{(1)}\left(x,h_1\right)=0\,,\ 0\le x<\infty\,, \tag{3}$$

$$\sigma_{yy}^{(1)}\left(x,h_1\right)=0\,,\ 0\le x<\infty\,, \tag{4}$$

$$\frac{\partial v^{(2)}\left(x,-h_2\right)}{\partial x}=0\,,\ \frac{\partial u^{(2)}\left(x,-h_2\right)}{\partial x}=0\,,\ 0\le x<\infty \tag{5}$$

$$\sigma_{yy}^{(1)}\left(x,0\right)=\sigma_{yy}^{(2)}\left(x,0\right)\,,\ 0\le x<\infty\,, \tag{6}$$

$$\tau_{xy}^{(1)}\left(x,0\right)=\sigma_{yy}^{(1)}\left(x,0\right)=0\,,\ 0\le x\le b\,. \tag{7}$$

Applying the Fourier integral transforms to equations (1) and (2):

$$\bar{u}\left(\alpha,y\right)=\int_0^\infty u\left(x,y\right)\sin\left(\alpha x\right)dx\,,\ \bar{v}\left(\alpha,y\right)=\int_0^\infty v\left(x,y\right)\cos\left(\alpha x\right)dx\,,$$

we obtain a system of ordinary differential equations. After finding the general solution of this system and applying the inverse Fourier transform,

$$u\left(x,y\right)=\frac{2}{\pi}\int_0^\infty \bar{u}\left(\alpha,y\right)\sin\left(\alpha x\right)d\alpha\,,\ v\left(x,y\right)=\frac{2}{\pi}\int_0^\infty \bar{v}\left(\alpha,y\right)\cos\left(\alpha x\right)d\alpha\,,$$

we will have

$$u^{(1)}\left(x,y\right)=\frac{2}{\pi}\int_0^\infty\left[\left(A_1+B_1y\right)e^{-\alpha y}+\left(C_1+D_1y\right)e^{\alpha y}\right]\sin\left(\alpha x\right)d\alpha\,, \tag{8}$$

$$v^{(1)}\left(x,y\right)=\frac{2}{\pi}\int_0^\infty\left[\left(A_1+\left(\frac{k_1}{\alpha}+y\right)B_1\right)e^{-\alpha y}+\left(-C_1+\left(\frac{k_1}{\alpha}-y\right)D_1\right)e^{\alpha y}\right]\cos\left(\alpha x\right)d\alpha\,, \tag{9}$$

$$u^{(2)}\left(x,y\right)=\frac{2}{\pi}\int_0^\infty\left[\left(A_2+B_2y\right)e^{-\alpha y}+\left(C_2+D_2y\right)e^{\alpha y}\right]\sin\left(\alpha x\right)d\alpha\,, \tag{10}$$

$$v^{(2)}\left(x,y\right)=\frac{2}{\pi}\int_0^\infty\left[\left(A_2+\left(\frac{k_2}{\alpha}+y\right)B_2\right)e^{-\alpha y}+\left(-C_2+\left(\frac{k_2}{\alpha}-y\right)D_2\right)e^{\alpha y}\right]\cos\left(\alpha x\right)d\alpha\,, \tag{11}$$

where A_1, B_1, C_1, D_1, A_2, B_2, C_2, D_2 are unknown constants.

Using the equations (8)–(11) and applying Hook's law we obtain

$$\tau_{xy}^{(1)}(x,y)=\frac{4\mu_1}{\pi}\int_0^\infty\left\{\left[-\alpha\left(A_1+B_1y\right)-B_1\frac{\kappa_1-1}{2}\right]e^{-\alpha y}+\right.$$
$$\left.+\left[\alpha\left(C_1+D_1y\right)-D_1\frac{\kappa_1-1}{2}\right]e^{\alpha y}\right\}\sin(\alpha x)\,d\alpha=0,$$
$$\tau_{xy}^{(2)}(x,y)=\frac{4\mu_2}{\pi}\int_0^\infty\left\{\left[-\alpha\left(A_2+B_2y\right)-B_2\frac{\kappa_2-1}{2}\right]e^{-\alpha y}+\right.$$
$$\left.+\left[\alpha\left(C_2+D_2y\right)-D_2\frac{\kappa_2-1}{2}\right]e^{\alpha y}\right\}\sin(\alpha x)\,d\alpha=0, \qquad (12)$$

$$\sigma_{yy}^{(1)}(x,y)=\frac{4\mu_1}{\pi}\int_0^\infty\left\{\left[-\alpha\left(A_1+B_1y\right)-B_1\frac{1+\kappa_1}{2}\right]e^{-\alpha y}+\right.$$
$$\left.+\left[-\alpha\left(C_1+D_1y\right)+D_1\frac{1+\kappa_1}{2}\right]e^{\alpha y}\right\}\cos(\alpha x)\,d\alpha=0,$$
$$\sigma_{yy}^{(2)}(x,y)=\frac{4\mu_2}{\pi}\int_0^\infty\left\{\left[-\alpha\left(A_2+B_2y\right)-B_2\frac{1+\kappa_2}{2}\right]e^{-\alpha y}+\right.$$
$$\left.+\left[-\alpha\left(C_2+D_2y\right)+D_2\frac{1+\kappa_2}{2}\right]e^{\alpha y}\right\}\cos(\alpha x)\,d\alpha=0. \qquad (13)$$

Let us introduce the unknown functions

$$f_1(x)=\frac{\partial u^{(1)}(x,0)}{\partial x}-\frac{\partial u^{(2)}(x,0)}{\partial x},\ f_2(x)=\frac{\partial v^{(1)}(x,0)}{\partial x}-\frac{\partial v^{(2)}(x,0)}{\partial x}\ \text{ for } 0\le x\le b. \qquad (14)$$

Then, by satisfying the boundary conditions (4)–(6) and equation (14), using (8)–(13), and applying the inverse Fourier transforms to the resulting equations, we arrive at the following system of linear algebraic equations with respect to where A_1, B_1, C_1, D_1, A_2, B_2, C_2, D_2:

$$-\alpha e^{-\alpha h_1}A_1+\left(-\alpha h_1-\frac{\kappa_1-1}{2}\right)e^{-\alpha h_1}B_1+\alpha e^{\alpha h_1}C_1+\left(\alpha h_1-\frac{\kappa_1-1}{2}\right)e^{\alpha h_1}D_1=0,$$

$$-\alpha e^{-\alpha h_1}A_1+\left(-\alpha h_1-\frac{\kappa_1+1}{2}\right)e^{-\alpha h_1}B_1-\alpha e^{\alpha h_1}C_1+\left(-\alpha h_1+\frac{\kappa_1+1}{2}\right)e^{\alpha h_1}D_1=\frac{P}{4\mu_1}\cos(\alpha a),$$

$$e^{\alpha h_2}A_2-h_2e^{\alpha h_2}B_2+e^{-\alpha h_2}C_2-h_2e^{-\alpha h_2}D_2=0,$$

$$e^{\alpha h_2}A_2+\left(\frac{\kappa_2}{\alpha}-h_2\right)e^{\alpha h_2}B_2-e^{-\alpha h_2}C_2+\left(\frac{\kappa_2}{\alpha}-h_2\right)e^{-\alpha h_2}D_2=0,$$

$$-\alpha KA_1 - K\frac{\kappa_1-1}{2}B_1 + \alpha KC_1 - \frac{\kappa_1-1}{2}KD_1 + \alpha A_2 + \frac{\kappa_2-1}{2}B_2 - \alpha C_2 + \frac{\kappa_2-1}{2}D_2 = 0,$$

$$A_1 + C_1 - A_2 - C_2 = \frac{1}{\alpha}\bar{f}_1(\alpha),$$

$$A_1 + \frac{\kappa_1}{\alpha}B_1 - C_1 + \frac{\kappa_1}{\alpha}D_1 - A_2 - \frac{\kappa_2}{\alpha}B_2 + C_2 - \frac{\kappa_2}{\alpha}D_2 = \frac{1}{\alpha}\bar{f}_2(\alpha),$$

where

$$K = \frac{\mu_1}{\mu_2},\ \bar{f}_2(\alpha) = \int_0^\infty f_2(x)\sin(\alpha x)dx,\ \bar{f}_1(\alpha) = \int_0^\infty f_1(x)\cos(\alpha x)dx.$$

The solution to this system was obtained using the computer algebra system Wolfram Mathematica 13.1, and based on it, the expressions for the stresses along the interface were found in the following form:

$$\tau_{xy}^{(1)}(x,0) = \frac{4\mu_1}{\pi}\int_0^\infty \left[H_{11}(\alpha)\bar{f}_1(\alpha) + H_{12}(\alpha)\bar{f}_2(\alpha)\right]\sin(\alpha x)d\alpha, \tag{15}$$

$$\sigma_{yy}^{(1)}(x,0) = \frac{4\mu_1}{\pi}\int_0^\infty \left[H_{21}(\alpha)\bar{f}_1(\alpha) + H_{22}(\alpha)\bar{f}_2(\alpha)\right]\cos(\alpha x)d\alpha, \tag{16}$$

where the functions $H_{ij}(\alpha)$ are provided in the appendix.

By evaluating $H_{ij}^\infty = H_{ij}(\alpha)$ at $\alpha \to \infty$, we can rewrite expressions (15) and (16) as:

$$\begin{aligned}\tau_{xy}^{(1)}(x,0) = {} & \frac{4\mu_1}{\pi}\int_0^\infty \left[\tilde{H}_{11}(\alpha)\bar{f}_1(\alpha) + \tilde{H}_{12}(\alpha)\bar{f}_2(\alpha)\right]\sin(\alpha x)d\alpha + \\ & + \frac{4\mu_1}{\pi}\int_0^\infty \left[H_{11}^\infty\,\bar{f}_1(\alpha) + H_{11}^\infty\,\bar{f}_2(\alpha)\right]\sin(\alpha x)d\alpha,\end{aligned} \tag{17}$$

$$\begin{aligned}\sigma_{yy}^{(1)}(x,0) = {} & \frac{4\mu_1}{\pi}\int_0^\infty \left[\tilde{H}_{21}(\alpha)\bar{f}_1(\alpha) + \tilde{H}_{22}(\alpha)\bar{f}_2(\alpha)\right]\cos(\alpha x)d\alpha + \\ & + \frac{4\mu_1}{\pi}\int_0^\infty \left[H_{21}^\infty\,\bar{f}_1(\alpha) + H_{22}^\infty\,\bar{f}_2(\alpha)\right]\cos(\alpha x)d\alpha,\end{aligned} \tag{18}$$

where

$$\tilde{H}_{ij}(\alpha) = H_{ij}(\alpha) - H_{ij}^\infty,\ H_{11}^\infty = H_{22}^\infty = -\frac{1+K+\kappa_1+\kappa_2 K}{\Delta},$$

$$H_{12}^{\infty}=H_{21}^{\infty}=\frac{1-K-\kappa_1+\kappa_2 K}{\Delta},\ \Delta=2\left(K+\kappa_1\right)\left(1+\kappa_2 K\right).$$

Considering the following integral formulas:

$$\int_0^{\infty}e^{-\eta\alpha}\sin\alpha\left(x\mp y\right)d\alpha=\frac{1}{x\mp y}\ \text{for}\ \eta\to 0,$$

$$\int_0^{\infty}f_i\left(t\right)\int_0^{\infty}\sin\left(\alpha t\right)\sin\left(\alpha x\right)d\alpha dt=\frac{\pi}{2}f_i\left(x\right),\ i=1,2,$$

and taking into account the symmetry relative to the axis *y*, the expressions for the stresses (17), (18), can be represented in the following form:

$$\begin{aligned}\tau_{xy}^{(1)}\left(x,0\right)&=\frac{2\mu_1}{\pi}\int_{-b}^{b}f_1\left(t\right)\int_0^{\infty}\tilde{H}_{11}\left(\alpha\right)\left[-\sin\alpha\left(t-x\right)\right]d\alpha dt+\\&+\frac{2\mu_1}{\pi}\int_{-b}^{b}f_2\left(t\right)\int_0^{\infty}\tilde{H}_{12}\left(\alpha\right)\cos\alpha\left(t-x\right)d\alpha dt-2\mu_1\left[H_{11}^{\infty}\frac{1}{\pi}\int_{-b}^{b}\frac{f_1\left(t\right)}{t-x}dt-H_{12}^{\infty}f_2\left(x\right)\right],\end{aligned}\tag{19}$$

$$\begin{aligned}\sigma_{yy}^{(1)}\left(x,0\right)&=\frac{2\mu_1}{\pi}\int_{-b}^{b}f_1\left(t\right)\int_0^{\infty}\tilde{H}_{21}\left(\alpha\right)\cos\alpha\left(t-x\right)d\alpha dt-\\&2\mu_1\left[H_{21}^{\infty}f_1\left(x\right)+H_{22}^{\infty}\frac{1}{\pi}\int_{-b}^{b}\frac{f_2\left(t\right)}{t-x}dt\right]\\&+\frac{2\mu_1}{\pi}\int_{-b}^{b}f_2\left(t\right)\int_0^{\infty}\tilde{H}_{22}\left(\alpha\right)\left[\sin\alpha\left(t-x\right)\right]d\alpha dt.\end{aligned}\tag{20}$$

Introducing the designations:

$$M_{11}\left(x,t\right)=\int_0^{\infty}\tilde{H}_{11}\left(\alpha\right)\sin\alpha\left(t-x\right)d\alpha,\ M_{12}\left(x,t\right)=\int_0^{\infty}\tilde{H}_{12}\left(\alpha\right)\cos\alpha\left(t-x\right)d\alpha,$$

$$M_{21}\left(x,t\right)=\int_0^{\infty}\tilde{H}_{21}\left(\alpha\right)\cos\alpha\left(t-x\right)d\alpha,\ M_{22}\left(x,t\right)=\int_0^{\infty}\tilde{H}_{22}\left(\alpha\right)\sin\alpha\left(t-x\right)d\alpha,$$

formulas (20) can be written in the following form:

$$\frac{\tau_{xy}^{(1)}\left(x,0\right)}{2\mu_1}=-\frac{H_{11}^{\infty}}{\pi}\int_{-b}^{b}\frac{f_1\left(t\right)}{t-x}dt+H_{12}^{\infty}f_2\left(x\right)-\frac{1}{\pi}\int_{-b}^{b}f_1\left(t\right)M_{11}\left(x,t\right)dt+\frac{1}{\pi}\int_{-b}^{b}f_2\left(t\right)M_{12}\left(x,t\right)dt,\tag{21}$$

$$\frac{\sigma_{yy}^{(1)}\left(x,0\right)}{2\mu_1}=-H_{21}^{\infty}f_1\left(x\right)-\frac{H_{22}^{\infty}}{\pi}\int_{-b}^{b}\frac{f_2\left(t\right)}{t-x}dt+\frac{1}{\pi}\int_{-b}^{b}f_1\left(t\right)M_{21}\left(x,t\right)dt+\frac{1}{\pi}\int_{-b}^{b}f_2\left(t\right)M_{22}\left(x,t\right)dt.\tag{22}$$

Satisfying further the boundary conditions (7), we arrive at the following system of singular integral equations:

$$-\frac{H_{11}^{\infty}}{\pi}\int_{-b}^{b}\frac{f_1(t)}{t-x}dt+H_{12}^{\infty}f_2(x)-\frac{1}{\pi}\int_{-b}^{b}f_1(t)M_{11}(x,t)\,dt+\frac{1}{\pi}\int_{-b}^{b}f_2(t)M_{12}(x,t)\,dt=0, \tag{23}$$

$$-H_{21}^{\infty}f_1(x)-\frac{H_{22}^{\infty}}{\pi}\int_{-b}^{b}\frac{f_2(t)}{t-x}dt+\frac{1}{\pi}\int_{-b}^{b}f_1(t)M_{21}(x,t)\,dt+\frac{1}{\pi}\int_{-b}^{b}f_2(t)M_{22}(x,t)\,dt=\frac{p_0}{2\mu_1}. \tag{24}$$

The additional conditions for this system are as follows:

$$\int_{-b}^{b}f_1(t)dt=0,\ \int_{-b}^{b}f_2(t)dt=0. \tag{25}$$

The solution of the system (23), (24) has an oscillatory singularity near the crack tips, but according to [15], for determining the global fracture parameters and the energy release rate (ERR), the oscillation can be neglected, and the solution of this system can be found in the form:

$$f_i(t)=\frac{f_i^*(t)}{\sqrt{b^2-t^2}},\ i=1,2. \tag{26}$$

Substituting (26) into (23)–(25) and transitioning to the interval $[-1,1]$ using the substitution $x=br$, $t=bs$, we obtain:

$$-\frac{H_{11}^{\infty}}{\pi}\int_{-1}^{1}\frac{\psi_1^*(s)\,ds}{(s-r)\sqrt{1-s^2}}+\frac{H_{12}^{\infty}\psi_2^*(r)}{\sqrt{1-r^2}}-\frac{b}{\pi}\int_{-1}^{1}\left[M_{11}(x,t)\frac{\psi_1^*(s)}{\sqrt{1-s^2}}-M_{12}(x,t)\frac{\psi_2^*(s)}{\sqrt{1-s^2}}\right]dt=0, \tag{27}$$

$$-\frac{H_{21}^{\infty}\psi_1^*(r)}{\sqrt{1-r^2}}-\frac{H_{22}^{\infty}}{\pi}\int_{-1}^{1}\frac{\psi_2^*(s)\,ds}{(s-r)\sqrt{1-s^2}}+\frac{b}{\pi}\int_{-1}^{1}\left[M_{21}(x,t)\frac{\psi_1^*(s)}{\sqrt{1-s^2}}+M_{22}(x,t)\frac{\psi_2^*(s)}{\sqrt{1-s^2}}\right]dt=\frac{p_0}{2\mu_1}, \tag{28}$$

$$\int_{-1}^{1}\frac{\psi_1^*(s)}{\sqrt{1-s^2}}dt=0,\ \int_{-1}^{1}\frac{\psi_2^*(s)}{\sqrt{1-s^2}}dt=0, \tag{29}$$

where $\psi_1^*(s)=f_1^*(bs)$, $\psi_2^*(s)=f_2^*(bs)$.

Consider the equations (27), (28) at the nodes $r_i=\cos\left(\frac{\pi i}{N}\right)$, $i=1,...,N-1$, and apply the Gauss-Chebyshev quadrature formula for calculating the integrals:

$$\int_{-1}^{1}\frac{\psi_m^*(s)}{\sqrt{1-s^2}}ds=\sum_{k=1}^{N}\frac{\pi}{N}\psi_m^*(s_k), \tag{30}$$

where $s_k=\cos\left(\frac{2k-1}{2N}\pi\right)$, $k=1,...,N$,

we arrive at the system:

$$-\frac{H_{11}^{\infty}}{N}\sum_{k=1}^{N}\frac{\psi_1^*(s_k)}{s_k-r_i}+H_{12}^{\infty}\frac{\psi_2^*(r_i)}{\sqrt{1-r_i^2}}-\frac{b}{N}\sum_{k=1}^{N}\left[M_{11}(x_i,t_k)\psi_1^*(s_k)-M_{12}(x_i,t_k)\psi_2^*(s_k)\right]=0,$$

$$-H_{21}^{\infty}\frac{\psi_1^*(r_i)}{\sqrt{1-r_i^2}}-\frac{H_{22}^{\infty}}{N}\sum_{k=1}^{N}\frac{\psi_2^*(s_k)}{s_k-r_i}+\frac{b}{N}\sum_{k=1}^{N}\left[M_{21}(x_i,t_k)\psi_1^*(s_k)+M_{22}(x_i,t_k)\psi_2^*(s_k)\right]=\frac{p_0}{2\mu_1}, \quad (31)$$

where $x_i=br_i$, $t_k=bs_k$, $i=1,...,N-1$.

Since the nodes r_k are between the nodes s_k and s_{k+1}, we find $\psi_m^*(r_k)$ through $\psi_m^*(s_k)$ and $\psi_m^*(s_{k+1})$ using linear interpolation:

$$\psi_m^*(r_k)=\frac{(r_k-s_{k+1})}{s_k-s_{k+1}}\psi_m^*(s_k)+\frac{(r_k-s_k)}{s_{k+1}-s_k}\psi_m^*(s_{k+1}),\ m=1,2. \quad (32)$$

Substituting (32) into (31), we obtain:

$$\begin{gathered}-\frac{H_{11}^{\infty}}{N}\sum_{k=1}^{N}\frac{\psi_1^*(s_k)}{s_k-r_i}+\sum_{k=1}^{N}\frac{H_{12}^{\infty}}{\sqrt{1-r_k^2}}\left[\delta_{i,k}\frac{(r_k-s_{k+1})}{s_k-s_{k+1}}\psi_2^*(s_k)+\delta_{i,k+1}\frac{(r_k-s_k)}{s_{k+1}-s_k}\psi_2^*(s_{k+1})\right]-\\-\frac{b}{N}\sum_{k=1}^{N}\left[M_{11}(x_i,t_k)\psi_1^*(s_k)+M_{12}(x_i,t_k)\psi_2^*(s_k)\right]=0.\end{gathered} \quad (33)$$

$$\begin{gathered}-\sum_{k=1}^{N}\frac{H_{21}^{\infty}}{\sqrt{1-r_k^2}}\left[\delta_{i,k}\frac{(r_k-s_{k+1})}{s_k-s_{k+1}}\psi_1^*(s_k)+\delta_{i,k+1}\frac{(r_k-s_k)}{s_{k+1}-s_k}\psi_1^*(s_{k+1})\right]-\frac{H_{22}^{\infty}}{N}\sum_{k=1}^{N}\frac{\psi_2^*(s_k)}{s_k-r_i}+\\+\frac{b}{N}\sum_{k=1}^{N}\left[M_{21}(x_i,t_k)\psi_1^*(s_k)+M_{22}(x_i,t_k)\psi_2^*(s_k)\right]=\frac{p_0}{2\mu_1},\end{gathered} \quad (34)$$

where $\delta_{i,k}$ are the Kronecker symbols, $i=1,...,N-1$.

Applying the quadrature formula (30) to the equations (29), we obtain:

$$\sum_{k=1}^{N}\psi_1^*(s_k)=0,\ \sum_{k=1}^{N}\psi_2^*(s_k)=0. \quad (35)$$

Equations (33)-(35) represent a system of $2N$ linear algebraic equations with $2N$ unknowns $\psi_1^*(s_k)$ and $\psi_2^*(s_k)$ ($k=1,2...,N$).

After solving the system, we obtain:

$$f_m(bs_k)=\frac{f_m^*(bs_k)}{b\sqrt{1-s_k^2}},\ m=1,2;\quad k=1,...,N.$$

Then, based on (14), the derivatives of the displacement jumps $f_1(x)$ and $f_2(x)$ at the upper and lower crack faces, are found. Using further the formulas:

$$\langle u(x,0)\rangle = \int_{-b}^{x} f_1(x)\,dx\,,\ \langle v(x,0)\rangle = \int_{-b}^{x} f_2(x)\,dx\,, \tag{36}$$

the displacement jumps:

$$\langle u(x,0)\rangle = u^{(1)}(x,0) - u^{(2)}(x,0) \text{ and } \langle v(x,0)\rangle = v^{(1)}(x,0) - v^{(2)}(x,0)$$

are determined.

To find the stresses, we use the formulas (21) and (22). However, considering that $f_1(x) = 0$ for $x \notin (-b,b)$, they take the following form:

$$\frac{\tau_{xy}^{(1)}(x,0)}{2\mu_1} = -\frac{H_{11}^{\infty}}{\pi}\int_{-b}^{b}\frac{f_1(t)}{t-x}dt - \frac{1}{\pi}\int_{-b}^{b} f_1(t)M_{11}(x,t)\,dt + \frac{1}{\pi}\int_{-b}^{b} f_2(t)M_{12}(x,t)\,dt\,,$$

$$\frac{\sigma_{yy}^{(1)}(x,0)}{2\mu_1} = -\frac{H_{22}^{\infty}}{\pi}\int_{-b}^{b}\frac{f_2(t)}{t-x}dt + \frac{1}{\pi}\int_{-b}^{b} f_1(t)M_{21}(x,t)\,dt + \frac{1}{\pi}\int_{-b}^{b} f_2(t)M_{22}(x,t)\,dt\,,\ x \notin (-b,b).$$

Performing an analysis similar to the outlined above, we arrive at the following formulas:

$$\frac{\tau_{xy}^{(1)}(x,0)}{2\mu_1} \approx -\frac{H_{11}^{\infty}}{N}\sum_{k=1}^{N}\frac{\psi_1^*(s_k)}{s_k - r} - \frac{b}{N}\sum_{k=1}^{N}\left[M_{11}(x,t_k)\psi_1^*(s_k) - M_{12}(x,t_k)\psi_2^*(s_k)\right], \tag{37}$$

$$\frac{\sigma_{yy}^{(1)}(x,0)}{2\mu_1} \approx -\frac{H_{22}^{\infty}}{N}\sum_{k=1}^{N}\frac{\psi_2^*(s_k)}{s_k - r} + \frac{b}{N}\sum_{k=1}^{N}\left[M_{21}(x,t_k)\psi_1^*(s_k) + M_{22}(x,t_k)\psi_2^*(s_k)\right], \tag{38}$$

where $x \notin (-b,b)$, $r = x/b$.

According to [15], the energy release rate G during the crack propagation can be calculated by the formula:

$$G = \frac{\pi b \mu_1}{\kappa_1 + 1}\hat{K}^2, \tag{39}$$

where $\hat{K} = \sqrt{\left[f_1^*(b)\right]^2 + \left[f_2^*(b)\right]^2}$.

3. RESULTS AND DISCUSSION

Numerical illustration of the obtained solution was carried out for a microcrack with a length of 2 μm and different thicknesses of two infinite layers in the range from 0,5 μm to

10 μm (Fig. 2, 3). Additionally, it was assumed that $\nu_1 = \nu_2 = 0,3$, the Young's modulus for each layer varies within the range from $2,2 \cdot 10^{-2}\ N/\mu m^2$ to $26 \cdot 10^{-2}\ N/\mu m^2$ and internal pressure $p_0 = 10^{-5}\ N/\mu m^2$.

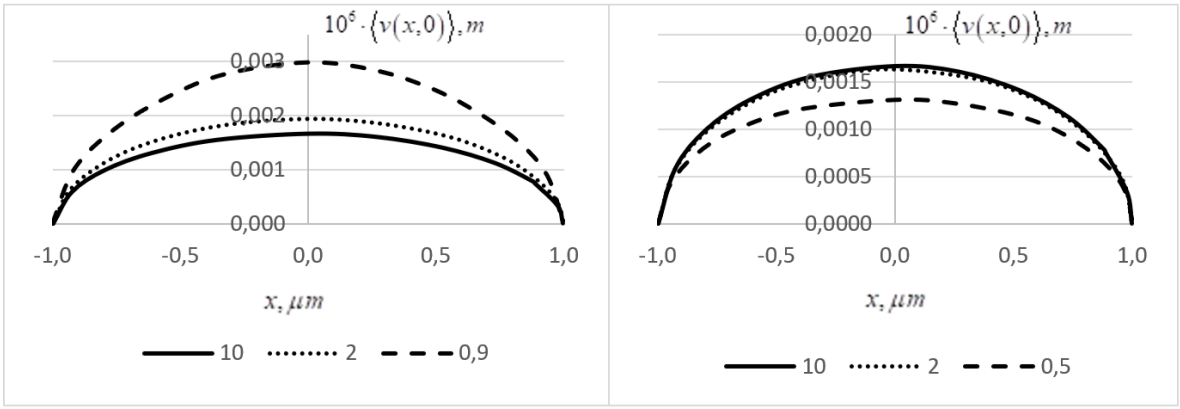

a) b)

Figure 2. Crack opening at:
a) $h_1 = 0,9–10\ \mu m$, $h_2 = 10\ \mu m$ ($E_1 = 0,026\ N/\mu m^2$, $E_2 = 0,022\ N/\mu m^2$)
b) $h_1 = 10\ \mu m$, $h_2 = 0,5–10\ \mu m$ ($E_1 = 0,026\ N/\mu m^2$, $E_2 = 0,022\ N/\mu m^2$)

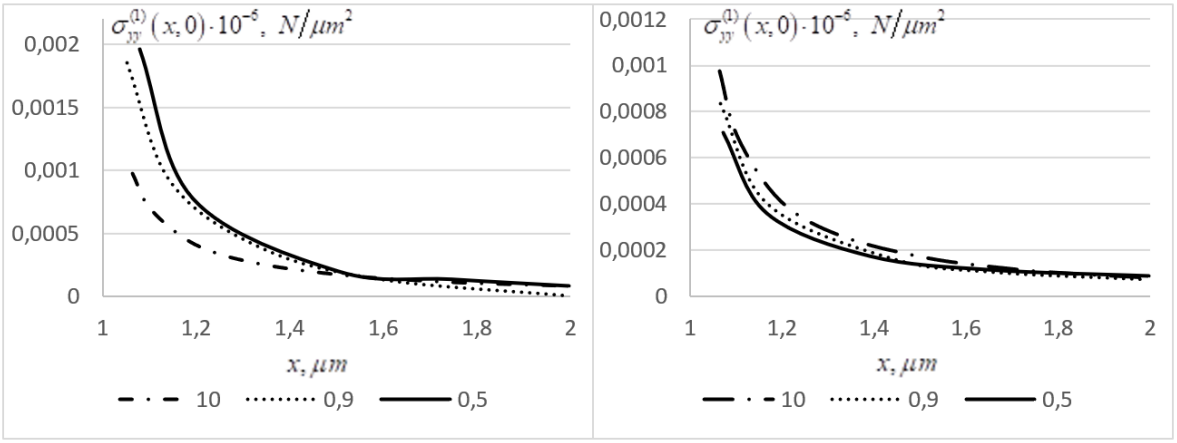

a) b)

Figure 3. The stress at the extension of the crack at:
a) $h_1 = 0,5–10\ \mu m$, $h_2 = 10\ \mu m$ ($E_1 = 0,026\ N/\mu m^2$, $E_2 = 0,022\ N/\mu m^2$)
б) $h_1 = 10\ \mu m$, $h_2 = 0,5–10\ \mu m$ ($E_1 = 0,026\ N/\mu m^2$, $E_2 = 0,022\ N/\mu m^2$)

It should be noted that as the thickness of the upper strip decreases, a significant increase in the crack opening and the energy release rate is observed (Table 1). On the other hand, when the thickness of the lower strip decreases, a significant change is observed only for thicknesses smaller than 0.5 μm, which may indicate that the crack opening values are approaching the possible limit for the applicability of linear elasticity theory.

Table 1

The change in the energy release rate

The thickness of the upper strip h_1, μm	The thickness of the lower strip h_2, μm	ERR·10^{-8} $N \cdot m$, $E_1 = 0{,}026\ N/\mu m^2$, $E_2 = 0{,}022\ N/\mu m^2$	E_1, $N/\mu m^2$	E_2, $N/\mu m^2$	ERR·10^{-8} $N \cdot m$, $h_1 = 2\ \mu m$, $h_2 = 10\ \mu m$
10	10	2,77	0,026	0,022	3,68
5		2,89	0,052		4,13
2		3,68	0,13		6,27
0,9		6,94	0,26		9,88
0,5		15,1			
10	10	2,77	0,026	0,022	3,68
	5	2,76		0,044	1,98
	2	2,66		0,11	1,16
	0,9	2,32		0,22	0,93
	0,5	1,92			

Figure 4 presents graphs of crack opening with variations in Young's modulus for the upper and lower thin layers. An increase in Young's modulus values results in a decrease in crack opening. However, the energy release rate at the crack edge for the upper layer significantly increases in this case, whereas, with an increase in Young's modulus for the lower layer, there is a marked decrease in the energy release rate for the coating (Table 1).

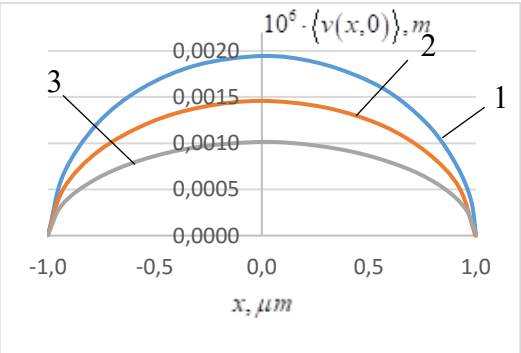

a) $h_1 = 2\ \mu m$, $h_2 = 10\ \mu m$ (1 – $E_1 = 0{,}026\ N/\mu m^2$, $E_2 = 0{,}022\ N/\mu m^2$; 2 – $E_1 = 0{,}052\ N/\mu m^2$, $E_2 = 0{,}022\ N/\mu m^2$; 3 – $E_1 = 0{,}26\ N/\mu m^2$, $E_2 = 0{,}022\ N/\mu m^2$)

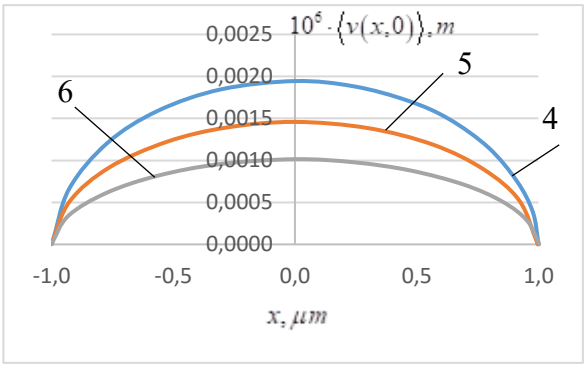

b) $h_1 = 2\ \mu m$, $h_2 = 10\ \mu m$ (4 – $E_1 = 0{,}026\ N/\mu m^2$, $E_2 = 0{,}022\ N/\mu m^2$; 5 – $E_1 = 0{,}026\ N/\mu m^2$, $E_2 = 0{,}044\ N/\mu m^2$; 6 – $E_1 = 0{,}026\ N/\mu m^2$, $E_2 = 0{,}22\ N/\mu m^2$)

Figure 4. Crack opening

For the case of a thin overlay of finite length, which is in contact with a thin strip of finite dimensions (Fig. 5), the analysis was conducted using the finite element method (FEM). A microcrack with a length of 2 μm was considered, with overlay and strip thicknesses in the range of 0,5−10 μm. Additionally, the parameters $L = 50\ \mu m$, $l = 50\ \mu m$. Other relevant values were chosen $\nu = 0{,}3$, $E_1 = 0{,}026\text{-}0{,}26\ N/\mu m^2$, $E_2 = 0{,}022\text{-}0{,}22\ N/\mu m^2$, $p_0 = 10 \cdot 10^{-6}\ N/\mu m^2$.

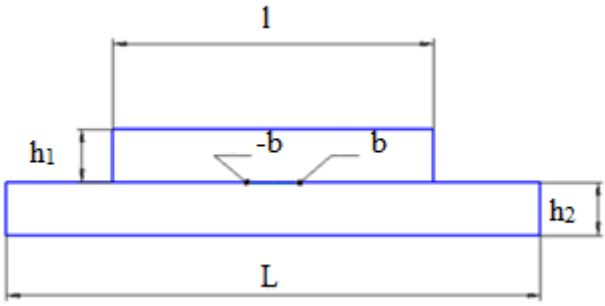

Figure 5. Thin overlay for FEM analysis

In the FEM modeling, the mesh refineent was performed in the vicinity of the crack (Fig. 6). The degree of refinement, as well as the element size, was varied depending on the overlay thickness.

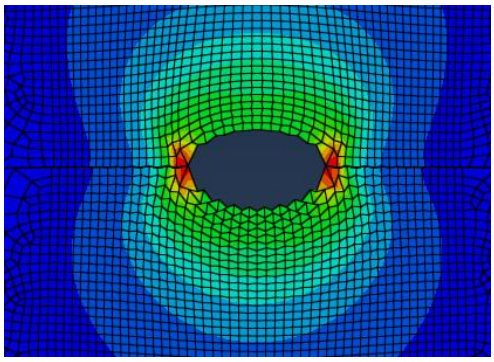

Figure 6. An example of a mesh with the distribution of von Mises stresses at $h_1 = 5\ \mu m$, $h_2 = 10\ \mu m$ ($E_1 = 0{,}026\ N/\mu m^2$, $E_2 = 0{,}022\ N/\mu m^2$)

The obtained distributions of stresses, crack opening, and energy release rate for different values of the characteristics of the thin overlay and strip are presented. For the case where the thickness of the overlay is half that of the strip, and the stiffnesses are approximately equal, a comparison between the analytical and numerical results was conducted (Fig. 7).

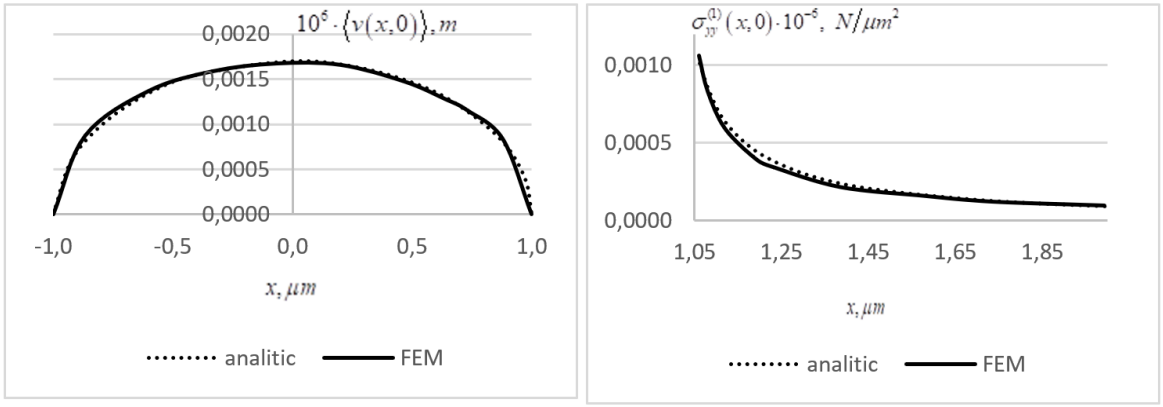

a) b)

Figure 7. A comparative analysis of the crack opening (a) and the stress at the extension of the crack (b) at: $h_1 = 5\ \mu m$, $h_2 = 10\ \mu m$ ($E_1 = 0{,}026\ N/\mu m^2$, $E_2 = 0{,}022\ N/\mu m^2$)

The presented graphs demonstrate good agreement between the results obtained using the analytical method and FEM. Both analytical and numerical methods were used to analyze the change in the crack opening shape with varying overlay and strip thicknesses, or changes in material stiffness, as well as the variations in the energy release rate depending on the changes in the thicknesses of the overlay and strip.

4. CONCLUSIONS

This work investigated the plane deformation of a crack located between two isotropic, linearly elastic, infinite layers, with the lower layer fixed rigidly. The crack is subjected to uniform internal pressure, and the crack opening and stress state were determined by solving the corresponding boundary value problem. Using Fourier integral transforms, a system of differential equations was constructed, from which analytical expressions were derived for the stresses and displacements in the layers.

Additionally, a numerical analysis was conducted using the finite element method (FEM) to verify the analytical results. Excellent agreement was found between the analytical and FEM results. Numerical calculations showed a significant influence of the upper layer's thickness on the crack opening and energy release rate; these parameters increase with decreasing upper layer thickness. It is therefore important to account for this effect in practical problems involving crack formation in multilayer materials.

These detailed results will contribute to the development of more fracture-resistant composites, especially in microelectronics applications, where microcracks can compromise device reliability.

References

1. Hu K. Q., Jin H., Yang Z., Chen X. (2019) Interface crack between dissimilar one-dimensional hexagonal quasicrystals with piezoelectric effect. Acta Mechanica, 230, pp. 2455–2474. https://doi.org/10.1007/s00707-019-02404-z
2. Pei P., Yang G., Shi Y., Gao C.-F. (2020) Periodic interfacial cracks in dissimilar piezoelectric materials under the influence of Maxwell stress. Meccanica, 55, pp. 113–124. https://doi.org/10.1007/s11012-019-01110-3
3. Verma P. R. (2022) Magnetic-yielding zone model for assessment of two mode-III semi-permeable collinear cracks in piezo-electro-magnetic strip. Mechanics of Advanced Materials and Structures, 29, pp. 1529–1542. https://doi.org/10.1080/15376494.2020.1827466
4. Hu K. Q., Gao C-F., Zhong Z., Chen Z. T. (2021) Interaction of collinear interface cracks between dissimilar one-dimensional hexagonal piezoelectric quasicrystals. Journal of Applied Mathematics and Mechanics, 101 (11). https://doi.org/10.1002/zamm.202000360
5. Onopriienko O. D., Govorukha V. B., Kagadii T. S., Shporta A. H. (2023) Analysis of cracks and shielding effects in modern materials. Computer Science and Applied Mathematics, 2, pp. 59–95. [in Ukrainian].
6. Erdogan F., Gupta G. D. (1971) Layered composites with an interface flaw. International Journal of Solids and Structures, no. 7, pp. 1089–1107. https://doi.org/10.1016/0020-7683(71)90082-5
7. Delale F., Erdogan F. (1983) The crack problem for a nonhomogeneous plane. Journal of Applied Mechanics, , 50, pp. 609–614. https://doi.org/10.1115/1.3167098
8. Delale F., Erdogan F. (1988) Interface crack in a nonhomogeneous elastic medium. International Journal of Engineering Science, 26 (6), pp. 559–568. https://doi.org/10.1016/0020-7225(88)90054-7
9. Birinci A., Birinci F., Cakiroglu F. L., Erdol R. (2010) An internal crack problem for an infinite elastic layer. Archive of Applied Mechanics, 80, pp. 997–1005. https://doi.org/10.1007/s00419-009-0355-5
10. Sheveleva A., Loboda V., Lapusta Y. (2020) A conductive crack and a remote electrode at the nterface between two piezoelectric materials. Applied Mathematical Modeling, 87, pp. 287–299. https://doi.org/10.1016/j.apm.2020.06.003
11. Loboda V., Lapusta Y., Sheveleva A. (2006) Analysis of pre-fracture zones for an electrically permeable crack in an interlayer between piezoelectric materials. International Journal of Fracture, 142 (3–4), pp. 307–313. https://doi.org/10.1007/s10704-006-9034-5

12. Kryven V., Kaplun A. (2014) Development of plastic areas in angle points zone under concentrated force. Scientific Journal of TNTU, 76 (4), pp. 34–43. (Mechanics and materials science).
13. Yasniy P., Dyvdyk O., Semenets O., Iasnii V., Antonov A. (2020) Fatigue crack growth in aluminum alloy from cold expanded hole with preexisting crack. Scientific Journal of TNTU, 99 (3), pp. 5–16. https://doi.org/10.33108/visnyk_tntu2020.03.005
14. Kryven V., Blashchak N., Valiashek V., Kryva N., Tsymbaliuk L. (2019) Elastic-plastic deformation of a half-layer with a notch at rigid loading. Scientific Journal of TNTU, 96 (4), pp. 5–13. https://doi.org/10.33108/visnyk_tntu2019.04.005
15. Zhang A. B., Wang B. L. (2013) An opportunistic analysis of the interface crack based on the modified interface dislocation method. International Journal of Solids and Structures, 50, pp. 15–20. https://doi.org/10.1016/j.ijsolstr.2012.08.024

Appendix

Expressions for the functions $H_{ij}(\alpha)$:

$$H_{11}[\alpha]=\frac{1}{Zn[\alpha]}\Big(-4e^{-2\alpha h_2}\alpha(1+\kappa_1)\left(1+e^{2\alpha h_2}\kappa_2\right)h_1\left(e^{2\alpha h_2}+\kappa_2-2\alpha h_2\right)+$$
$$+4e^{-2\alpha h_2}\left(-1+e^{2\alpha h_2}\right)K\alpha^2(1+\kappa_2)h_1^2\left(\kappa_2+e^{2\alpha h_2}\kappa_2-2\alpha h_2\right)+$$
$$+4\sinh[\alpha h_1]\Big(-\left((1+\kappa_1)\cosh[\alpha h_1]\left(1+\kappa_2{}^2+2\kappa_2\cosh[2\alpha h_2]\right)\right)-2K\kappa_2(1+\kappa_2)\sinh[\alpha h_1]\sinh[2\alpha h_2]+$$
$$+2\alpha\Big((1+\kappa_1)\left(e^{-2\alpha h_2}+\kappa_2\right)\cosh[\alpha h_1]+\left(1-e^{-2\alpha h_2}\right)K(1+\kappa_2)\sinh[\alpha h_1]\Big)h_2\Big)\Big);$$

$$H_{12}[\alpha]=\frac{1}{Zn[\alpha]}\Big(2\left(-1+\kappa_1-2K\kappa_2+\left(-1+2K+\kappa_1\right)\kappa_2{}^2\right)-2\left(-1+\kappa_1-2K\kappa_2+\left(-1+2K+\kappa_1\right)\kappa_2{}^2\right)\cosh[2\alpha h_1]-$$
$$-2\kappa_2\left(-1+K+\kappa_1-K\kappa_2\right)\cosh\left[2\alpha\left(h_1-h_2\right)\right]+\kappa_2\left(4\left(-1+K+\kappa_1-K\kappa_2\right)\cosh[2\alpha h_2]+\right.$$
$$\left.+\left(-2\left(-1+K+\kappa_1\right)+K\kappa_2\right)\cosh\left[2\alpha\left(h_1+h_2\right)\right]+K\kappa_2(\cosh\left[\alpha\left(2h_1+h_2\right)\right]+\sinh\left[2\alpha\left(h_1+h_2\right)\right]-\sinh\left[\alpha\left(2h_1+h_2\right)\right])\right)+$$
$$+2\alpha\Big(\Big(2K+e^{-2\alpha(h_1+h_2)}\left(-1+K+\kappa_1\right)-e^{-\alpha(2h_1+h_2)}K\kappa_2-2\left(-1+K+\kappa_1\right)\kappa_2+e^{2\alpha(h_1-h_2)}\left(-1+K+\kappa_1-K\kappa_2\right)-$$
$$-2e^{-2\alpha h_2}\left(-1+K+\kappa_1-K\kappa_2\right)+e^{-2\alpha h_1}\left(-K+\left(-1+K+\kappa_1\right)\kappa_2\right)+e^{2\alpha h_1}\left(-K+\left(-1+K+\kappa_1\right)\kappa_2\right)\Big)h_2+$$
$$+2e^{-2\alpha h_2}\alpha h_1^2\left(-e^{4\alpha h_2}\left(2+K\left(-1+\kappa_2\right)\right)\kappa_2-\left(2+K\left(-1+\kappa_2\right)\right)\left(\kappa_2-2\alpha h_2\right)-\right.$$
$$\left.-2e^{2\alpha h_2}\left(1+\kappa_2\left(K+\kappa_2-K\kappa_2\right)+\alpha\left(-K+\left(-2+K\right)\kappa_2\right)h_2\right)\right)\Big);$$

$$H_{21}(\alpha)=\frac{1}{Zn[\alpha]}\Big(-4\left(-1+\kappa_1-2K\kappa_2+\left(-1+2K+\kappa_1\right)\kappa_2{}^2+2\kappa_2\left(-1+K+\kappa_1-K\kappa_2\right)\cosh[2\alpha h_2]\right)\sinh[\alpha h_1]^2+$$
$$+4e^{-2\alpha h_2}\alpha\Big(2\left(-1+K+\kappa_1-K\kappa_2+e^{2\alpha h_2}\left(K+\left(-1+3K+\kappa_1\right)\kappa_2\right)\right)\sinh[\alpha h_1]^2h_2+$$
$$+\alpha h_1^2\left(-e^{4\alpha h_2}\left(2+K\left(-1+\kappa_2\right)\right)\kappa_2-\left(2+K\left(-1+\kappa_2\right)\right)\left(\kappa_2-2\alpha h_2\right)-\right.$$
$$\left.-2e^{2\alpha h_2}\left(1+\kappa_2\left(K+\kappa_2-K\kappa_2\right)+\alpha\left(K-2\kappa_2+3K\kappa_2\right)h_2\right)\right)\Big);$$

$$H_{22}(\alpha)=\frac{1}{Zn[\alpha]}\Big(4\Big(e^{-2\alpha h_2}\alpha(1+\kappa_1)\left(1+e^{2\alpha h_2}\kappa_2\right)h_1\left(e^{2\alpha h_2}+\kappa_2-2\alpha h_2\right)+$$
$$+e^{-2\alpha h_2}\left(1+e^{2\alpha h_2}\right)K\alpha^2(1+\kappa_2)h_1^2\left(\left(-1+e^{2\alpha h_2}\right)\kappa_2+2\alpha h_2\right)+$$
$$+\sinh[\alpha h_1]\Big(-\left((1+\kappa_1)\cosh[\alpha h_1]\left(1+\kappa_2{}^2+2\kappa_2\cosh[2\alpha h_2]\right)\right)-2K\kappa_2(1+\kappa_2)\sinh[\alpha h_1]\sinh[2\alpha h_2]+$$
$$+2\alpha\Big((1+\kappa_1)\left(e^{-2\alpha h_2}+\kappa_2\right)\cosh[\alpha h_1]+\left(-1-e^{-2\alpha h_2}\right)K(1+\kappa_2)\sinh[\alpha h_1]\Big)h_2\Big)\Big),$$

where

$$Zn[\alpha] = 8K\alpha^2\left(1+\kappa_1\right)\left(1+\kappa_2\right)h_1h_2 -$$
$$-8\mathrm{e}^{-2\alpha h_2}\alpha^2\left(-1+\mathrm{e}^{2\alpha h_2}\left(-1+K\right)\kappa_2 - K\kappa_2\right)h_1^2\left(\kappa_2 - K\kappa_2 + \mathrm{e}^{2\alpha h_2}\left(1+K\kappa_2\right)+2\left(-1+K\right)\alpha h_2\right)+$$
$$+2\mathrm{e}^{-2\alpha\left(h_1+h_2\right)}\left(1-\mathrm{e}^{2\alpha h_2}\left(-1+K\right)\kappa_2 + K\kappa_2 + \mathrm{e}^{2\alpha\left(h_1+h_2\right)}\left(K+\kappa_1\right)\kappa_2 + \mathrm{e}^{2\alpha h_1}\left(\kappa_1 - K\kappa_2\right)\right)\times$$
$$\times\left(-\mathrm{e}^{2\alpha h_1}\left(-1+K\right)\kappa_2 + \left(K+\kappa_1\right)\kappa_2 + \mathrm{e}^{2\alpha h_2}\left(\kappa_1 - K\kappa_2\right) + \mathrm{e}^{2\alpha\left(h_1+h_2\right)}\left(1+K\kappa_2\right)+2\alpha\left(\mathrm{e}^{2\alpha h_1}\left(-1+K\right)-K-\kappa_1\right)h_2\right).$$

УДК 539.3

ОСОБЛИВОСТІ ДЕФОРМУВАННЯ ДВОХ ТОНКИХ ПОЛОС З МІКРОТРІЩИНОЮ НА МЕЖІ ЇХ З'ЄДНАННЯ

Олександр Клєцков[1]; Валентина Сіліч-Балгабаєва[1]; Алла Шевельова[1]; Володимир Лобода[1]; Юрій Лапуста[2]

[1]Дніпровський національний університет імені Олеся Гончара
[2]Клермонський університет, інженерна школа Оверні, SIGMA Клермон, Національний центр наукових досліджень, Інститут Паскаля, Клермон-Ферран, F-63000, Франція.

Резюме. *Детально розглянуто задачу про плоску деформацію тріщини, що знаходиться між двома ізотропними, лінійно пружними шарами, один з яких жорстко закріплений. Для розв'язання цієї задачі було використано метод інтегральних перетворень Фур'є, який дозволив звести початкову систему диференціальних рівнянь у частинних похідних до системи звичайних диференціальних рівнянь. На її основі побудовано систему сингулярних інтегральних рівнянь (СІР), яка задовольняє крайові умови задачі. Ця система описує напруженно-деформований стан біматеріальної полоси з тріщиною. Для розв'язання системи сингулярних інтегральних рівнянь застосовано метод дискретизації. Суть методу полягає в тому, що неперервна система рівнянь замінюється на дискретну, що дозволяє отримати наближений розв'язок. У даному випадку дискретизація призвела до системи лінійних алгебраїчних рівнянь (СЛАР).*

Розв'язавши систему лінійних алгебраїчних рівнянь, отримано вирази для розкриття тріщини та розподілу напружень на межі поділу матеріалів. Ці результати є ключовими для аналізу механічної поведінки тріщини та оцінювання її впливу на конструкцію.

На основі отриманих даних про розкриття тріщини та розподіл напружень було обчислено швидкість звільнення енергії (ШЗЕ) у вершинах тріщини. ШЗЕ є важливим параметром, який характеризує енергетичний стан тріщини та її схильність до росту. Для ілюстрації отриманих результатів проведено чисельне моделювання. Зокрема, побудовано графіки розкриття тріщини та залежності напружень для різних товщин шарів і модулів Юнга. Ці графіки демонструють вплив геометричних та матеріальних параметрів на поведінку тріщини.

Отримані аналітичні розв'язки порівняно з чисельними розв'язками, отриманими методом скінченних елементів (МСЕ). Порівняння показало гарне узгодження результатів для випадку мікротріщини при змінних значеннях характеристик тонкої накладки та нижнього шару.

Особливу увагу приділено дослідженню впливу товщини накладки на швидкість звільнення енергії. Виявлено значний вплив цього параметра на ШЗЕ, що підкреслює важливість його врахування при проектуванні багатошарових конструкцій.

Проведене дослідження дозволяє отримати детальну інформацію про механічну поведінку тріщини, розташованої між двома ізотропними шарами. Отримані результати можна використати для прогнозування розвитку тріщин та оцінювання міцності конструкцій.

Ключові слова: *мікротріщина, напружено-деформівний стан, сингулярні інтегральні рівняння, швидкість звільнення енергії, розкриття тріщини.*

https://doi.org/10.33108/visnyk_tntu2025.02.153 *Отримано 14.03.2025*